

LETTER • OPEN ACCESS

Simulation of the dipole pattern of summer precipitation over the Tibetan Plateau by CMIP6 models

To cite this article: Wei Shang *et al* 2021 *Environ. Res. Lett.* **16** 014047

View the [article online](#) for updates and enhancements.

You may also like

- [Large scale climate oscillation impacts on temperature, precipitation and land surface phenology in Central Asia](#)
Kirsten M de Beurs, Geoffrey M Henebry, Braden C Owsley et al.
- [\(Invited\) High-Yield and Long-Lived Triplet Excited States of Pentacene Alkanethiolate Monolayer Protected Gold Nanoparticles By Singlet Fission](#)
Taku Hasobe and Hayato Sakai
- [Recent interdecadal changes in the interannual variability of precipitation and atmospheric circulation over northern Eurasia](#)
Tetsuya Hiyama, Hatsuki Fujinami, Hironari Kanamori et al.

ENVIRONMENTAL RESEARCH
LETTERS

LETTER

Simulation of the dipole pattern of summer precipitation over the Tibetan Plateau by CMIP6 models

OPEN ACCESS

RECEIVED

23 September 2020

REVISED


23 November 2020

ACCEPTED FOR PUBLICATION

4 December 2020

PUBLISHED

11 January 2021

Wei Shang¹, Keqin Duan¹, Shuangshuang Li¹, Xuejuan Ren² and Bo Huang³ ¹ School of Geography and Tourism, Shaanxi Normal University, Xi'an, People's Republic of China² CMA-NJU Joint Laboratory for Climate Prediction Studies, School of Atmospheric Sciences, Nanjing University, Nanjing, People's Republic of China³ Industrial Ecology Programme, Department of Energy and Process Engineering, Norwegian University of Science and Technology, Trondheim, NorwayE-mail: kqduan@snnu.edu.cn

Original content from this work may be used under the terms of the [Creative Commons Attribution 4.0 licence](https://creativecommons.org/licenses/by/4.0/).

Any further distribution of this work must maintain attribution to the author(s) and the title of the work, journal citation and DOI.

**Keywords:** summer precipitation, Tibetan Plateau, CMIP6, North Atlantic oscillation, moisture transportSupplementary material for this article is available [online](#)**Abstract**

The dipole pattern of summer precipitation over the Tibetan Plateau (TP) during 1961–2014 is evaluated based on observations and 18 models provided by the Coupled Model Intercomparison Project Phase 6. Of the 18 models, 10 can capture the opposite variation characteristics in the south and north TP. Observational data reveals that the south–north seasaw of TP summer precipitation is essentially driven by a Rossby wave propagating from the Western Europe to East Asia, which is associated with North Atlantic oscillation (NAO). The models successfully simulated the dipole pattern that is closely related to the reproduction of the NAO–TP relationship. Further analysis demonstrates that the reliable simulations of horizontal dynamic processes of moisture transport, which is linked to the NAO–TP relationship, highly contributes to their success in reproducing the dipolar pattern of TP summer precipitation. While unrealistic local vertical circulation and evaporation simulation lead to the failed reproductions. These findings provide significant information for model development and future climate change projections.

1. Introduction

The Tibetan Plateau (TP), known as the ‘Third Pole of the world’, has a significant impact on global weather and climate systems through dynamic and thermal effects (Wu *et al* 2007). The TP is also the origin of many Asian rivers, e.g. the Yellow River, Yangtze River and Mekong River, leading to it being called the ‘Asian water tower’ (Xu *et al* 2008). The summer precipitation over the TP is abundant and accounts for more than half of the total annual rainfall changes in amount (Feng and Zhou 2012), and has experienced significant changes in recent decades (Yang *et al* 2014, Yao *et al* 2019). The variations of the TP precipitation are critically important for the hydrological cycle and ecology balance. Thus, it is of great significance to understand the mechanisms and moisture transport processes of the summer TP precipitation.

The summer precipitation of TP dominantly shows an antiphase between the south and north TP at interannual variability (Liu and Yin 2001, Liu *et al*

2015). The variation of summer TP precipitation is not only influenced by the Asian monsoon circulation, but also affected by the teleconnection associated with the North Atlantic Ocean as well as the North Atlantic oscillation (NAO), the Pacific Ocean and the Indian Ocean (Bothe *et al* 2010, Gao *et al* 2013, Hu *et al* 2016, Sun *et al* 2020). Wang *et al* (2017) revealed that the interannual variation of precipitation over the south TP is related to the moisture from western boundary and is primarily modulated by westerlies and strong NAO. With respect to atmospheric moisture transport, many studies have documented the different moisture sources of the TP and their variations on different timescales (Curio *et al* 2015, Dong *et al* 2016, Zhang *et al* 2017a, Zhou *et al* 2019). Zhang *et al* (2019) examined that in terms of climatology, the moisture in the north TP mainly came from Europe, whereas that in the south TP is associated with the Indian Ocean. Furthermore, the summer TP precipitation is dominantly explained by the dynamic process of atmospheric moisture budget,

which is due to circulation changes, and less attribute to the thermodynamic process that is associated with specific humidity anomalies (Gao *et al* 2014, Wang *et al* 2017, Zhang *et al* 2017b).

Global coupled climate models have been extensively explored to understand variations in climate systems and to project future climate changes. Based on the Coupled Model Intercomparison Project phase 5 (CMIP5), global climate models have many discrepancies for precipitation simulation. For instance, CMIP5 models overestimate the annual mean precipitation over the TP, especially for the southeastern regions (Chen and Frauenfeld 2014, Jiang *et al* 2016, Yue *et al* 2016). Furthermore, only half of the CMIP5 models could capture the observed seasonal pattern of TP precipitation (Su *et al* 2013, Hu *et al* 2014). The seesaw pattern between the TP precipitation and East Asian summer monsoon, which is observed on inter-annual timescale, is also poorly reproduced (Duan *et al* 2013). The large biases of CMIP5 models regarding TP precipitation may be linked to the coarse resolution, subgrid-scale physics, inaccurate simulation of circulation and complex terrains (Duan *et al* 2013, Zhang and Li 2016, Chen *et al* 2017, Salunke *et al* 2019). Recently, CMIP6 has issued the outputs simulated by state-of-the-art models in the worldwide. Most CMIP6 models have improved model resolution, optimized physical schemes, and included additional biochemical process in the earth system (Eyring *et al* 2016). More advanced models are provided to achieve more reliable precipitation simulations and future projections (Chen *et al* 2020, Park *et al* 2020, Zhu *et al* 2020). However, few works have focused on the simulation of TP regions. Therefore, it is of great necessity to evaluate the performance of CMIP6 models in reproducing the TP precipitation, particularly the interannual variation in summer.

In this study, we examined the simulation of interannual dipolar pattern of summer TP precipitation in CMIP6 models. Then, how well the CMIP6 models capture the teleconnection relationship between the summer TP precipitation and NAO is discussed. The physical process associated with atmospheric moisture budget is also diagnosed. The aim of this study is to assess the ability of CMIP6 models in reproducing the variability of summer TP precipitation and the underlying physical processes, which provides useful insights into model development and future climate changes projection.

2. Data and methods

2.1. Datasets

The datasets used included the following: (a) monthly precipitation grid dataset of $0.5^\circ \times 0.5^\circ$ horizontal resolution for the period of 1961–2014, distributed across TP regions provided by the Climate Data Center, China Meteorological Administration. (b) Monthly reanalysis data for geopotential height,

wind, vertical velocity, specific humidity and evaporation on $2.5^\circ \times 2.5^\circ$ horizontal resolution for 1961–2014 period, obtained from the National Center for Atmospheric Research (NCEP/NCAR) (Kalnay *et al* 1996), and $1^\circ \times 1^\circ$ horizontal resolution in 1979–2014 period provided by the European Center for Medium-Range Weather Forecasts (ERA-Interim, Dee *et al* 2011). The observational and reanalysis datasets are called ‘observation’ in the present study. (c) The monthly historical simulation for 18 CMIP6 models from 1961–2014 is used in this study. The model outputs are interpolated into the same resolution to compare with the observation datasets. More detail information for the 18 CMIP6 models is in table 1 and can also be found at <https://esgf-node.llnl.gov/search/cmip6/>.

2.2. Atmospheric moisture budget analysis

The regional precipitation is generally connected with evaporation and moisture transport. The anomalous moisture budget (Chou *et al* 2009, Seager *et al* 2010) is expressed as follows:

$$P' = E' - \partial_t \langle q \rangle' - \langle \mathbf{V} \cdot \nabla_h q \rangle' - \langle \omega \partial_p q \rangle', \quad (1)$$

where q is the specific humidity, P is the precipitation, E is the evaporation, \mathbf{V} is the horizontal wind vector (u, v), ω is the vertical pressure velocity. $\langle \rangle$ represents a vertical integration from surface to 300 hPa. The time variation of specific humidity term $\partial_t \langle q \rangle'$ can be neglected on the seasonal mean timescale.

A variable is decomposed into its time mean (overbar) and interannual anomalies (prime) and non-interannual components, the anomalous inter-annual moisture transport term in (1) can be expressed as:

$$-\langle \mathbf{V} \cdot \nabla_h q \rangle' = -\langle \mathbf{V}' \cdot \nabla_h \bar{q} \rangle - \langle \bar{\mathbf{V}} \cdot \nabla_h q' \rangle - \langle \mathbf{V}' \cdot \nabla_h q' \rangle + \text{residue}, \quad (2)$$

$$-\langle \omega \partial_p q \rangle' = -\langle \omega' \partial_p \bar{q} \rangle - \langle \bar{\omega} \partial_p q' \rangle - \langle \omega' \partial_p q' \rangle + \text{residue}, \quad (3)$$

where term $-\langle \mathbf{V} \cdot \nabla_h q \rangle'$ and term $-\langle \omega \partial_p q \rangle'$ represent the horizontal and vertical moisture advection. The dynamic terms in horizontal and vertical are $-\langle \mathbf{V}' \cdot \nabla_h \bar{q} \rangle$ and $-\langle \omega' \partial_p \bar{q} \rangle$. The thermodynamic terms are $-\langle \bar{\mathbf{V}} \cdot \nabla_h q' \rangle$ and $-\langle \bar{\omega} \partial_p q' \rangle$, respectively. Residue is represent the nonlinear interaction part. Term $-\langle \mathbf{V}' \cdot \nabla_h q' \rangle$, $-\langle \omega' \partial_p q' \rangle$ and residue are very small terms and, hence, are ignored in this study.

3. Results

3.1. Dipole pattern of Tibetan summer precipitation in CMIP6 models

Figure 1(a) plots the first empirical orthogonal function (EOF) pattern of the observation. It

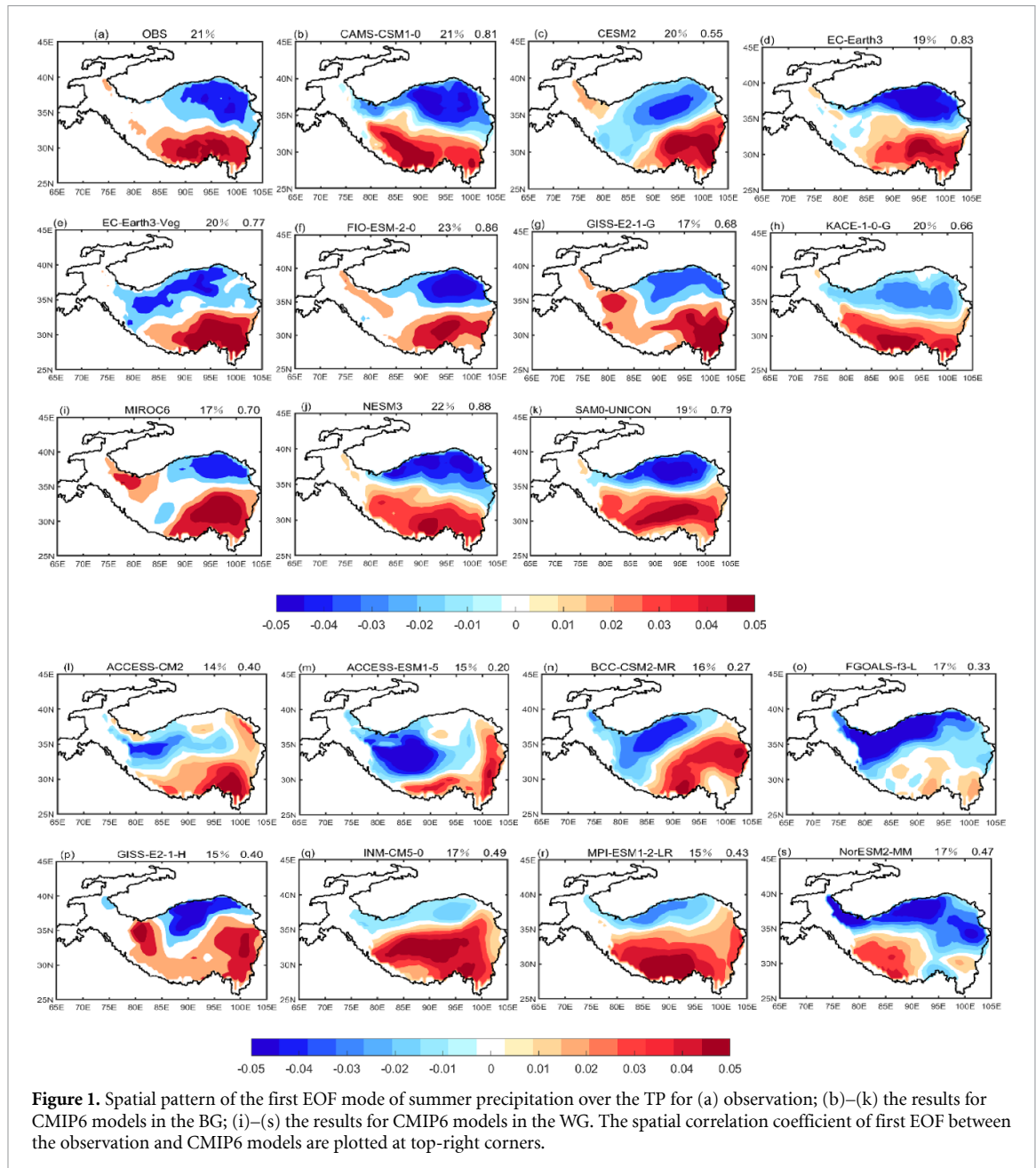
Table 1. Model name, institute ID, latitude and longitude numbers of each model used in this study.

| No. | Model name | Model full name | Institution ID | Lat × Lon |
|-----|---------------|-----------------------------------------------------------------------------------------|------------------------|-----------|
| 1 | ACCESS-CM2 | Australian Community Climate and Earth System Simulator | CSIRO/Australia | 144 × 192 |
| 2 | ACCESS-ESM1-5 | Earth Systems Model version of ACCESS | CSIRO/Australia | 144 × 192 |
| 3 | BCC-CSM2-MR | Beijing Climate Center Climate System Model | BCC/China | 160 × 320 |
| 4 | CAMS-CSM1-0 | The Climate System Model of the Chinese Academy of Meteorological Sciences | CAMS/China | 160 × 320 |
| 5 | CESM2 | Community Earth System Model version 2 | NCAR/USA | 192 × 288 |
| 6 | EC-Earth3 | European community Earth-System Model | EC-Earth-Consortium/EU | 256 × 512 |
| 7 | EC-Earth3-Veg | European community Earth-System Model with interactive vegetation module | EC-Earth-Consortium/EU | 256 × 512 |
| 8 | FGOALS-f3-L | Flexible Global Ocean-Atmosphere-Land System model | CAS/China | 180 × 288 |
| 9 | FIO-ESM-2-0 | First Institute of Oceanography Earth System Model version 2.0 | FIO-QLNM/China | 192 × 288 |
| 10 | GISS-E2-1-G | Goddard Institute for Space Studies Earth System Model-G | NASA-GISS/USA | 90 × 144 |
| 11 | GISS-E2-1-H | Goddard Institute for Space Studies Earth System Model-H | NASA-GISS/USA | 90 × 144 |
| 12 | INM-CM5-0 | Russian Institute for Numerical Mathematics Climate Model Version 5 | INM/Russia | 120 × 180 |
| 13 | KACE-1-0-G | Korea Meteorological Administration Advanced Community Earth-system model | KMA/Korea | 144 × 192 |
| 14 | MIROC6 | MIROC Consortium model version 6 | MIROC/Japan | 128 × 256 |
| 15 | MPI-ESM1-2-LR | Max Planck Institute Earth System Model-LR | MPI-M/Germany | 96 × 192 |
| 16 | NESM3 | Nanjing University of Information Science and Technology Earth System Model version 3.0 | NUIST/China | 96 × 192 |
| 17 | NorESM2-MM | Norwegian Earth System Model version 2MM | NCC/Norway | 192 × 288 |
| 18 | SAM0-UNICON | Seoul National University Atmosphere Model version 0 with a Unified Convection Scheme | SNU/Korea | 192 × 288 |

demonstrates a dipole pattern in the south and north TP with a 21% variance being explained. The EOF1 pattern of the CMIP6 models are shown in figures 1(b) and (s). There are large differences among the CMIP6 models and the variances range between 14% and 23%. According to the pattern correlation coefficients of EOF1 between the observation and models, the models can be categorized into two groups. (a) Better group (BG) models, with correlation coefficients larger than 0.5, comprising CAMS-CSM1-0, CESM2, EC-Earth3, EC-Earth3-Veg, FIO-ESM-2-0, GISS-E2-1-G, KACE-1-0-G, MIROC6, NESM3, and SAM0-UNICON. (b) Worse group (WG) models, with pattern coefficients smaller than 0.5, involving ACCESS-CM2, ACCESS-ESM1-5, BCC-CSM2-MR, FGOALS-f3-L, GISS-E2-1-H, INM-CM5-0, MPI-ESM1-2-LR, and NorESM2-MM.

Besides the pattern correlation coefficients of EOF1, we also consider the latitude of the Tanggula Mountains separating the south and north TP at 33° N–34° N. All the BG models reproduce the dipole pattern and, in each model, the center of the pattern is located over the central-eastern TP, similar to observation. However, the EOF1 pattern shows strong differences across the WG models. For example, the centers are simulated in the western TP in ACCESS-CM2 and BCC-CSM2-MR, and the separating latitude is north of the Tanggula Mountains.

Figure 2 displays the variation of summer precipitation averaged over the south TP (27° N–33° N, 85° E–105° E) and north TP (34° N–39° N, 85° E–105° E) by each model and the ensemble means of the BG models (figure 2(a)) and WG models (figure 2(b)). Both the south and north



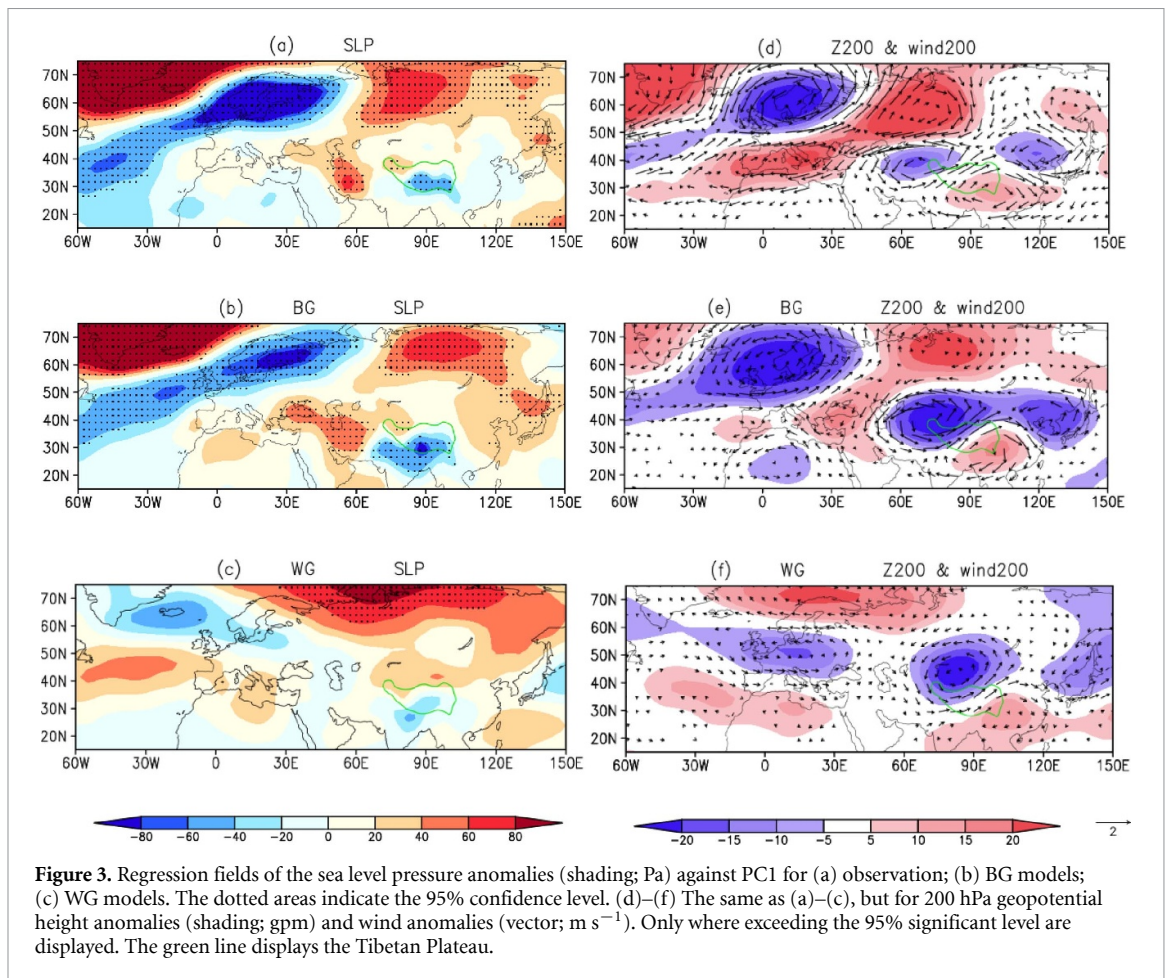
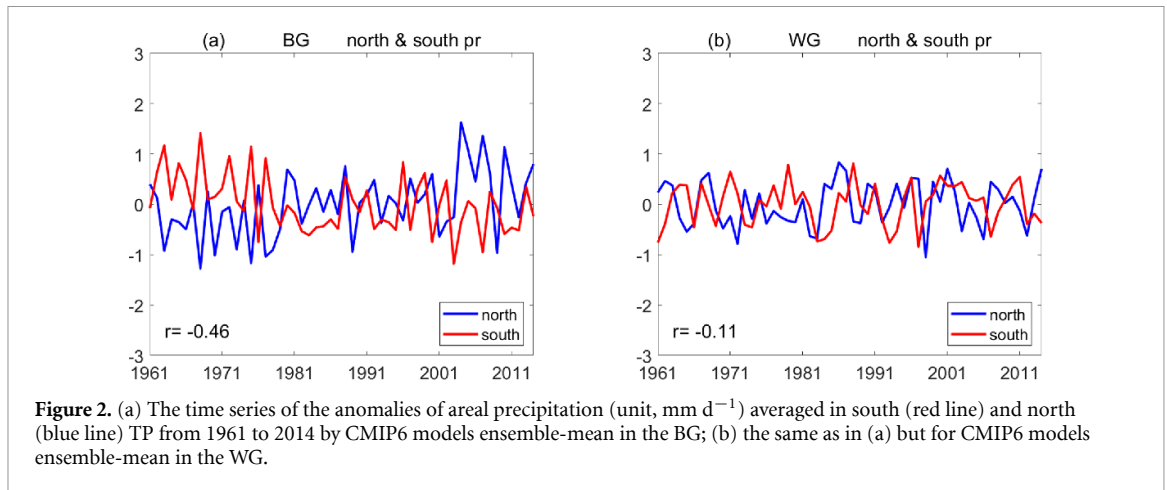
TP precipitation manifest an interannual variation during 1961–2014. In the BG models, the precipitation over the south TP and north TP demonstrates the opposite variation with a correlation coefficient of -0.46 , consistent with the EOF1 pattern. However, the correlation is only -0.11 for the WG models, much lower than the significant test. The results verify the well simulation of the dipole pattern of TP summer precipitation in the BG models.

3.2. Influence of the North Atlantic oscillation

The interannual variation of precipitation over the TP is dominantly influenced by the moisture transport from the western boundary, which is associated with the NAO (Gao *et al* 2013, Liu *et al* 2015, Wang *et al* 2017). In this section, we focus on the teleconnection between the NAO and TP precipitation variation and

assess the models' performance when simulating this relationship.

Figures 3(a) and (c) illustrate the regression fields of sea level pressure (SLP) anomalies against the PC1 (time series of principal component) of TP summer precipitation in observation, ensemble-mean BG models and WG models, respectively. In observation, there are high SLP anomalies in Iceland and low SLP anomalies in Azores. This north–south opposite pattern over the North Atlantic is related to the negative NAO phase (Watanabe *et al* 1999, Pan 2005). Meanwhile, low pressure anomalies manifest over the south TP, which favors the enhancement of local precipitation. The BG models could successfully reproduce the dipolar SLP pattern over the North Atlantic sector exactly consistent with the observation. However, in the WG models, the SLP anomalies are inverse to



the observation and BG models. Although weaker low anomalies appear in the TP, they may not be associated with the NAO.

To further demonstrate the impact of NAO on TP summer precipitation, figures 3(d) and (f) depict the regression anomalies of geopotential height and wind at 200 hPa against PC1. In observation, there is an evident Rossby wave train propagating from north-western Europe to southern TP, which resembles that stimulated by the negative NAO phase (Liu *et al* 2015, Wang *et al* 2017). Such wave train

causes a strong anticyclone over the south TP, enhancing the divergence in the upper troposphere and providing beneficial conditions for abnormal precipitation. This wave train connects the NAO and TP precipitation, suggesting the importance of western boundary downstream moisture transport. The regression anomalies of the SLP pattern and associated Rossby waves at 200 hPa are also clearly seen by using the ERA-interim reanalysis data for the observation (figure S1 (available online at stacks.iop.org/ERL/16/014047/mmedia)).

In the BG models, the Rossby wave related to NAO anomalies is closely similar to that of the observation, indicating the successful simulation of the NAO–TP relationship. In contrast, the wave trains in the WG models are much weaker and are not reproduced as the NAO phase.

In general, the BG models could simulate the dipolar SLP anomalies and Rossby waves associated with NAO anomalies, which contribute to reproduce the dipole pattern of TP precipitation. However, this process is not captured in the WG models. The above analysis confirms that the simulation of the dipole pattern of summer TP precipitation is exactly related to the reproduction of the teleconnection relationship between the NAO and TP.

A realistic NAO in terms of structure and variability may be vital for reproducing the TP summer precipitation pattern. Thus, we have checked the summer NAO pattern in the BG and WG models (figure S2). The spatial extent and intensity of the summer NAO are weaker than the winter NAO, and the center is located further north to the Western Europe (Folland *et al* 2009). In the BG model, the NAO pattern is well reproduced, which is similar to the observation. However, the SLP anomalies exhibit a tripolar pattern over North Atlantic regions in the WG models. That means the WG models fail to capture the summer NAO pattern, and thus the unrealistic impact of NAO on TP precipitation.

It is interesting to note that the weak low surface pressure and high pressure at 200 hPa in the WG models are also favorable for precipitation over TP. However, they are not related to NAO and downstream moisture transport. It also implies that the NAO may not be the only reason for the anomalous precipitation over TP. According to the moisture budget in equation (1), the regional precipitation anomalies may both be influenced by the remote moisture transport and local evaporation. For the dipole pattern of TP precipitation, the horizontal moisture transport is dominantly related to the NAO in observation and BG models. However, the unrealistic anomalous local circulation and evaporation could also cause the precipitation changes, which may affect the failed simulation in the dipole pattern of TP precipitation for the WG models. Further detailed analysis will be discussed in the next section.

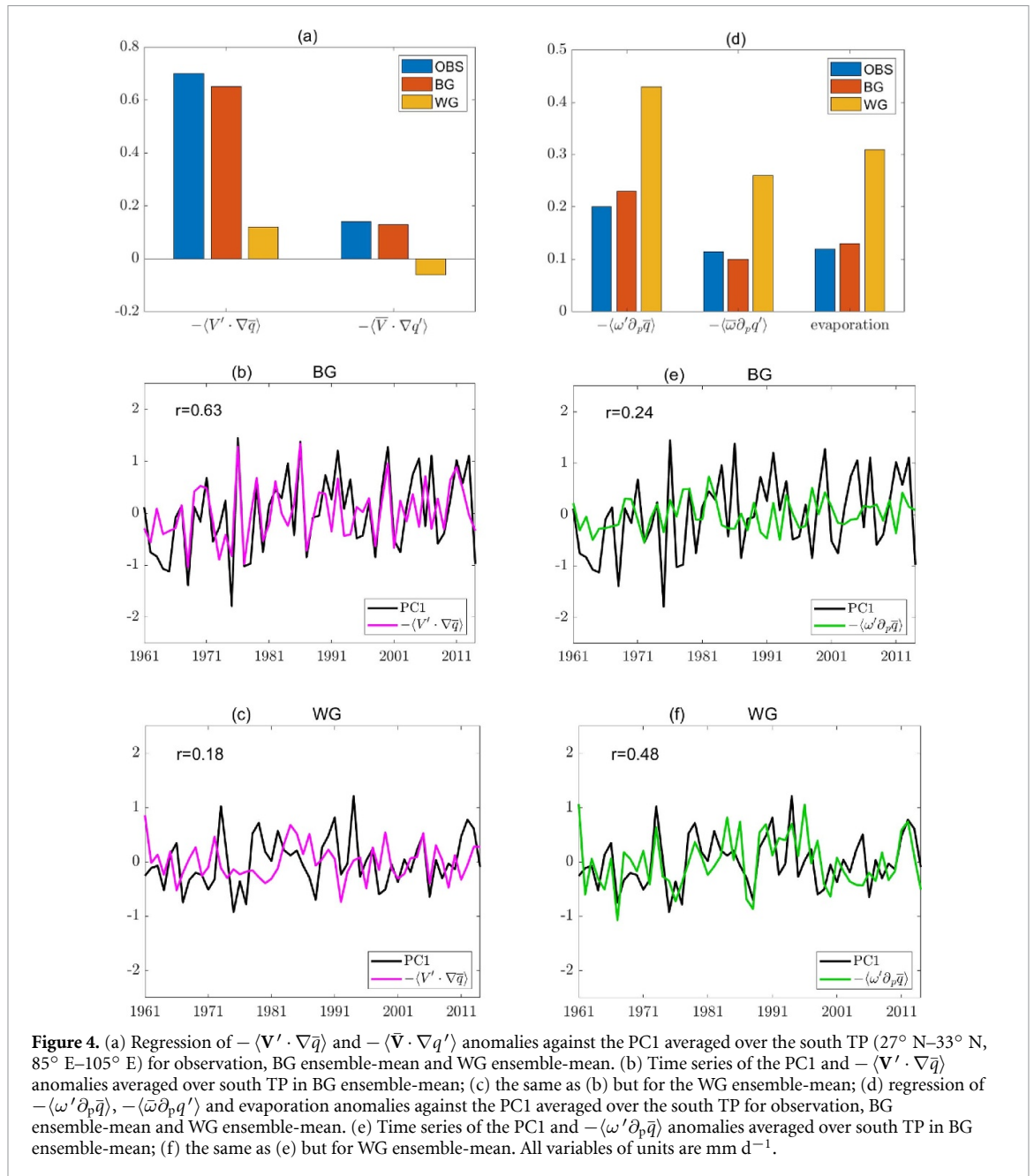
3.3. Diagnosis of atmospheric moisture budget

We diagnose the atmospheric moisture budget to demonstrate the dynamic and thermodynamic process contributions to the dipole TP summer precipitation. In observation, the dynamic component could explain large majority variance of the TP moisture transport, whereas the thermodynamic and evaporation contributions are much smaller on inter-annual timescale (Wang *et al* 2017, Zhang *et al* 2017a). This implies that the variations in atmo-

spheric circulation play a more important role in the water vapor transport of summer TP precipitation than the specific humidity changes.

Figure 4(a) shows the regression anomalies of the horizontal components of moisture convergence against PC1 averaged over the south TP (27° N–33° N, 85° E–105° E) for observation, BG ensemble-mean and WG ensemble-mean. In observation, the dipolar pattern of TP precipitation is dominated by the horizontal dynamic term ($-\langle \mathbf{V}' \cdot \nabla \bar{q} \rangle$), which is substantially linked to the NAO influence and western boundary moisture transport. The horizontal thermodynamic term ($-\langle \bar{\mathbf{V}} \cdot \nabla q' \rangle$) contributes much less to TP precipitation. Thus, we focus on the dynamic part of the moisture transport. In the BG models, the horizontal dynamic term resembles that of the observation. However, the WG models simulate much smaller values than the observation and BG models. In addition, the correlation between the ensemble-mean PC1 and horizontal dynamic term in the BG models can be reached to 0.63 at 99% significant level (figure 4(b)), while it is only 0.18 in the WG models (figure 4(c)). This suggests that the WG models could not accurately simulate the dynamic process of moisture transport related to the dipole pattern of TP precipitation, consistent with their inability to reproduce the NAO–TP relationship. Better simulation of the dynamic process indicates a realistic reproduction of atmosphere circulations affecting the water vapor transport, and thus the dipolar pattern of the TP summer precipitation.

The vertical components of moisture convergence and evaporation anomalies are given in figure 4(d). In the observation and BG models, the vertical process and evaporation anomalies have less impact on the water vapor transport than the horizontal moisture transport. In contrast, they are simulated to be much more significant in the WG models. Though the individual models may behave different performance, the WG models simulate much larger biases of local vertical circulation and evaporation anomalies, especially in the south TP regions (figures S3 and S4). The correlation between the ensemble-mean PC1 and vertical dynamic term ($-\langle \omega' \partial_p \bar{q} \rangle$) is only 0.24 in the BG models (figure 4(e)), while it is twice as large (0.48) in the WG model (figure 4(f)). Furthermore, the evaporation anomalies in the WG models also have larger deviation than those in observation and BG models, especially in the south TP regions. That means the major contribution of the TP precipitation anomalies in the WG models can be attributed to the anomalous local vertical circulation and evaporation. The large deviations in the horizontal and vertical dynamic components of moisture convergence suggest the false simulation in water vapor transport of the summer TP precipitation, which further affects the reproduction of precipitation over the south and north TP in the WG models.



4. Summary and discussion

The present study investigates the dipolar pattern of summer precipitation in TP regions based on the observations and 18 CMIP6 models. In observation, the summer precipitation in TP is characterized as an opposite variation in south and north TP. This dipolar pattern is primarily driven by Rossby wave trains propagating from the North Atlantic Ocean to East Asia. The wave trains cause an anomalous anticyclone in the upper troposphere, increasing the divergence, which favors for the precipitation in the south TP.

Of the 18 CMIP6 models, 10 can capture the dipole pattern of summer TP precipitation. According to the pattern correlation coefficient of EOF1 and the latitude of Tanggula Mountains, we divide the

models into two groups. The BG models could simulate a realistic dipole pattern that closely resembles to the observation, whereas it is not well reproduced in WG models. Further analysis reveals that the BG models capture the NAO–TP relationship as well as the wave trains from the Western Europe to East Asia. In contrast, the WG models fail to achieve this teleconnection.

The water vapor convergence is further discussed based on the atmosphere moisture budget. For observational data, the dynamic process largely contributes to the summer TP precipitation. The positive impact of dynamics process is reliable reproduced in the BG models. However, the WG models capture much weaker horizontal dynamic process. Further, the dramatic local vertical circulation and evaporation processes have more impact on the TP

precipitation in the WG models. Thus, the success of BG models reproducing the dipolar pattern of summer TP precipitation is attributed to the realistic simulation of the dynamic process associated with moisture transport. While the failure of the WG models is mainly related to the unrealistic local vertical circulation and evaporation simulation.

It is noted that the TP precipitation variation is complicated and changeable, and latent heating releasing from precipitation may influence the ‘pumping effect’ and related circulations (Wu et al 2017, He et al 2019). The moisture source of TP precipitation could be associated both with the westerlies and monsoon (Pan et al 2019, Zhang et al 2019, Zhou et al 2019). However, different mode variations of TP precipitation may have distinguished mechanisms at multi-timescales. Our findings emphasized the NAO–TP relationship, as well as the underlying horizontal dynamic moisture transport for the dipole pattern of summer TP precipitation at inter-annual timescale, both in observation and models. These findings are beneficial for understanding and developing the simulation of TP precipitation. The different abilities of BG and WG models in reproducing the dipole pattern of summer TP precipitation are also likely connected to the simulations of the interaction between atmosphere and land surface component. The development of land surface model (e.g. soil moisture transportation and land over phenology) may have potential to improve the coupled model performance in capturing the two items. Additionally, the resolutions of the global climate models are still rougher than the regional models, resulting in the complex terrain may be neglected. Thus, in order to simulate more detailed TP precipitation, the dynamic downscaling work needs to be taken into consideration in the future.

Data availability statement

All data that support the findings of this study are included within the article (and any supplementary files).

Acknowledgments

We thank anonymous reviewers for comments and suggestions that have substantially improved the manuscript. This work was jointly supported by the Second Tibetan Plateau Scientific Expedition and Research (STEP) program (Grant No. 2019QZKK0201), the National Natural Science Foundation of China (Grant Nos. 41571062, 41675067 and 41701592) and the Postdoctoral Science Foundation of China (Grant No. 2019M663616). The monthly precipitation data was provided by the China Meteorological Administration for academic use from <http://data.cma.cn/en/?r=data/index&cid=6d1b5efbdc9a58>. The

NCEP/NCAR monthly reanalysis data could be freely obtained from the website www.esrl.noaa.gov/psd/data/gridded/data.ncep.reanalysis.html. The ERA-Interim monthly reanalysis data could be freely downloaded from <https://apps.ecmwf.int/datasets/data/interim-full-mod/levtype=sfc/>. The CMIP6 model data was accessed from <https://esgf-node.llnl.gov/search/cmip6/>.

ORCID iD

Bo Huang  <https://orcid.org/0000-0001-6073-432X>

References

- Bothe O, Fraedrich K and Zhu X H 2010 Large-scale circulations and summer drought and wetness on the Tibetan Plateau *Int. J. Climatol.* **30** 844–55
- Chen L and Frauenfeld O W 2014 A comprehensive evaluation of precipitation simulations over China based on CMIP5 multi-model ensemble projections *J. Geophys. Res. Atmos.* **119** 5767–86
- Chen X Y, You Q L, Sielmann F and Ruan N 2017 Climate change scenarios for Tibetan Plateau summer precipitation based on canonical correlation analysis *Int. J. Climatol.* **37** 1310–21
- Chen Z M, Zhou T J, Zhang L X, Chen X L, Zhang W X and Jiang J 2020 Global land monsoon precipitation changes in CMIP6 projections *Geophys. Res. Lett.* **47** e2019GL086902
- Chou C, Neelin J D, Chen C-A and Tu J-Y 2009 Evaluating the ‘rich-get-richer’ mechanism in tropical precipitation change under global warming *J. Clim.* **22** 1982–2005
- Curio J, Maussion F and Scherer D 2015 A 12-year high-resolution climatology of atmospheric water transport over the Tibetan Plateau *Earth Syst. Dyn.* **6** 109–24
- Dee D P et al 2011 The ERA-Interim reanalysis: configuration and performance of the data assimilation system *Q. J. Meteorol. Soc.* **137** 553–97
- Dong W H et al 2016 Summer rainfall over the southwestern Tibetan Plateau controlled by deep convection over the Indian subcontinent *Nat. Commun.* **7** 10925
- Duan A M, Hu J and Xiao Z X 2013 The Tibetan Plateau summer monsoon in the CMIP5 simulations *J. Clim.* **26** 7747–66
- Eyring V, Bony S, Meehl G A, Senior C A, Stevens B, Stouffer R J and Taylor K 2016 Overview of the Coupled Model Intercomparison Project Phase 6 (CMIP6) experimental design and organization *Geosci. Model Dev.* **9** 1937–58
- Feng L and Zhou T J 2012 Water vapor transport for summer precipitation over the Tibetan Plateau: multidata set analysis *J. Geophys. Res.* **117** D20114
- Folland C K, Knight J, Linderholm H, Fereday D, Ineson S and Hurrell J W 2009 The summer North Atlantic oscillation: past, present, and future *J. Clim.* **22** 1082–103
- Gao Y, Wang H J and Li S L 2013 Influences of the Atlantic Ocean on the summer precipitation of the southeastern Tibetan Plateau *J. Geophys. Res. Atmos.* **118** 3534–44
- Gao Y H, Cuo L and Zhang Y X 2014 Changes in moisture flux over the Tibetan Plateau during 1979–2011 and possible mechanisms *J. Clim.* **27** 1876–93
- He C, Wang Z Q, Zhou T J and Li T 2019 Enhanced latent heating over the Tibetan Plateau as a key to the enhanced East Asian summer monsoon circulation under a warming climate *J. Clim.* **32** 3373–88
- Hu Q, Jiang D B and Fan G Z 2014 Evaluation of CMIP5 models over the Qinghai-Tibetan Plateau (Chinese with English abstract) *J. Geophys. Res. Atmos.* **38** 924–38
- Hu W T, Duan A M, Li Y and He B 2016 The intraseasonal oscillation of Eastern Tibetan Plateau precipitation in response to the summer Eurasian wave train *J. Clim.* **29** 7215–30

- Jiang D B, Tian Z P and Lang X M 2016 Reliability of climate models for China through the IPCC third to fifth assessment reports *Int. J. Climatol.* **36** 1114–33
- Kalnay E et al 1996 The NCEP/NCAR 40-year reanalysis project *Bull. Am. Meteorol. Soc.* **77** 437–71
- Liu H C, Duan K Q, Li M, Shi P H, Yang J, Zhang X and Sun J 2015 Impact of the North Atlantic oscillation on the dipole oscillation of summer precipitation over the central and eastern Tibetan Plateau *Int. J. Climatol.* **35** 4539–46
- Liu X D and Yin Z-Y 2001 Spatial and temporal variation of summer precipitation over the eastern Tibetan Plateau and the North Atlantic oscillation *J. Clim.* **14** 2896–909
- Pan C, Zhu B, Gao J H, Kang H Q and Zhu T 2019 Quantitative identification of moisture sources over the Tibetan Plateau and the relationship between thermal forcing and moisture transport *Clim. Dyn.* **52** 181–96
- Pan -L-L 2005 Observed positive feedback between the NAO and the North Atlantic SSTA tripole *Geophys. Res. Lett.* **32** L06707
- Park J, Kim H, Wang S-Y, Jeong J-H, Lim K-S, Lapante M and Yoon J-H 2020 Intensification of the East Asian summer monsoon lifecycle based on observation and CMIP6 *Environ. Res. Lett.* **15** 0940b9
- Salunke P, Jain S and Mishra S K 2019 Performance of the CMIP5 models in the simulation of the Himalaya-Tibetan Plateau monsoon *Theor. Appl. Climatol.* **137** 909–28
- Seager R, Naik N and Vecchi G A 2010 Thermodynamic and dynamic mechanisms for large-scale changes in the hydrological cycle in response to global warming *J. Clim.* **23** 4651–68
- Su F G, Duan X L, Chen D L, Hao Z H and Cuo L 2013 Evaluation of the global climate models in the CMIP5 over the Tibetan Plateau *J. Clim.* **26** 3187–208
- Sun J, Yang K, Guo W D, Wang Y, He J and Lu H 2020 Why has the inner Tibetan Plateau become wetter since the mid-1990s? *J. Clim.* **33** 8507–21
- Wang Z Q, Duan A M, Yang S and Ullah K 2017 Atmospheric moisture budget and its regulation on the variability of summer precipitation over the Tibetan Plateau *J. Geophys. Res. Atmos.* **122** 614–30
- Watanabe M, Kimoto M, Nitta T and Kachi M 1999 A comparison of decadal climate oscillations in the North Atlantic detected in observations and a coupled GCM *J. Clim.* **12** 2920–40
- Wu G X, He B, Duan A M, Liu Y M and Yu W 2017 Formation and variation of the atmospheric heat source over the Tibetan Plateau and its climate effects *Adv. Atmos. Sci.* **34** 1169–84
- Wu G X, Liu Y M, Wang T M, Wan R J, Liu X, Li W P, Wang Z Q, Zhang Q, Duan A M and Liang X Y 2007 The influence of the mechanical and thermal forcing of the Tibetan Plateau on the Asian climate *J. Hydrometeorol.* **8** 770–89
- Xu X D, Lu C G, Shi X H and Gao S T 2008 World water tower: an atmospheric perspective *Geophys. Res. Lett.* **35** L20815
- Yang K, Wu H, Qin J, Lin C G, Tang W J and Chen Y 2014 Recent climate changes over the Tibetan Plateau and their impacts on energy and water cycle: a review *Glob. Planet. Change* **112** 79–91
- Yao T D et al 2019 Recent third pole's rapid warming accompanies cryospheric melt and water cycle intensification and interactions between monsoon and environment: multidisciplinary approach with observations, modeling, and analysis *Bull. Am. Meteorol. Soc.* **100** 423–44
- Yue T X, Zhao N, Fan Z M, Li J, Chen C F, Lu Y M, Wang C L, Xu B and Wilson J 2016 CMIP5 downscaling and its uncertainty in China *Glob. Planet. Change* **146** 30–37
- Zhang C, Tang Q H and Chen D L 2017a Recent changes in the moisture source of precipitation over the Tibetan Plateau *J. Clim.* **30** 1807–19
- Zhang C, Tang Q, Chen D L, Ent R J V, Liu X C, Li W H and Haile G 2019 Moisture source changes contributed to different precipitation changes over the Northern and Southern Tibetan Plateau *J. Hydrometeorol.* **20** 217–29
- Zhang L and Li J 2016 Impact of moisture divergence on systematic errors in precipitation around the Tibetan Plateau in a general circulation model *Clim. Dyn.* **47** 2923–34
- Zhang W X, Zhou T J and Zhang L X 2017b Wetting and greening Tibetan Plateau in early summer in recent decades *J. Geophys. Res. Atmos.* **122** 5808–22
- Zhou C Y, Zhao P and Chen J M 2019 The interdecadal change of summer water vapor over the Tibetan Plateau and associated mechanisms *J. Clim.* **32** 4103–19
- Zhu H H, Jiang Z H, Li J, Li W, Sun C X and Li L 2020 Does CMIP6 inspire more confidence in simulating climate extremes over China? *Adv. Atmos. Sci.* **37** 1119–32